Sensors and Actuators A 323 (2021) 112643

Contents lists available at ScienceDirect

Sensors and Actuators A: Physical

journal homepage: www.elsevier.com/locate/sna

Nanowatt simple microcalorimetry for dynamically monitoring the defense mechanism of *Paramecium caudatum*

Jianguo Feng[a], Hanliang Zhu[a], Julius Lukeš[b], Marie Korabečná[c], Zdenka Fohlerová[d,f], Ting Mei[e], Honglong Chang[a,*], Pavel Neužil[a,d,f,*]

[a] School of Mechanical Engineering, Northwestern Polytechnical University, Xi'an, 710072, PR China
[b] Institute of Parasitology, Biology Centre, Czech Academy of Sciencesand Faculty of Sciences, University of South Bohemia, 370 05, České Budějovice, Czech Republic
[c] 1st Faculty of Medicine, Institute of Biology and Medical Genetics, Charles University, 128 00, Prague, Czech Republic
[d] Central European Institute of Technology, Brno University of Technology, 612 00, Brno, Czech Republic
[e] School of Natural and Applied Sciences, Northwestern Polytechnical University, Xi'an, 710129, PR China
[f] Brno University of Technology, Faculty of Electrical Engineering and Communication, Department of Microelectronics, Technicka 10, 616 00 Brno, Czech Republic

ARTICLE INFO

Article history:
Received 13 October 2020
Received in revised form 14 January 2021
Accepted 18 February 2021
Available online 24 February 2021

Keywords:
Microcalorimetry
Energy balance monitoring
Defense mechanism
Metabolic heat
Unicellular organism

ABSTRACT

Microcalorimetry has been widely used in measuring cellular metabolic heat to study bioprocesses, such as metabolism. However, it is still limited by insufficient sensitivity and system complexity, especially for the direct measurements of individual cells. Here, we present a droplet-based simple differential microcalorimetric system for determining the real-time energy balance of the ciliate protist, *Paramecium caudatum*. We utilized the platform to dynamically monitor its defensive behavior and measured the temperature change. Then we used heat balance equation and calculated corresponding dissipated power and energy with an ultimate resolution of ≈14 nW. The results showed that the defensive behavior by the ejection of the trichocysts' content consumed energy of ≈0.75 mJ per cell, and the dissipated power was ≈303.8 μW. This differential microcalorimetric platform can be used to study the metabolic heat of protist metabolism as well as other individual cells, helping us to understand this widespread, yet little-known, biological phenomenon from a new perspective.

1. Introduction

Real-time energy balance monitoring is crucial for characterizing and analyzing the thermodynamics of physical, chemical, and biological processes [1–5], with a special emphasis on unicellular eukaryotes, as well as individual cells from multicellular organisms [6]. These experiments provide a new type of information about general cellular processes, such as metabolism and responses to environmental stimuli [7]. There are several approaches that can be used to monitor their energy balance, including scanning thermal microscopy [8], fluorescent techniques based on fluorescent polymeric thermometers [9], green fluorescent protein [10] or quantum dots [11], and microcalorimetry for the overall reaction heat measurements [12]. Microcalorimetry has become a powerful tool for characterizing label-free molecular interactions by evaluating their enthalpy [13,14]. It is capable of processing small volume samples in or even below the μL range, leading to a high thermal resolution. Therefore, it has been widely used to monitor the energy balance and measure the metabolic heat of bioprocesses in cells and tissues [3,4,15,16], perform disease diagnosis [17] and aid in drug discovery [18–20]. However, monitoring the energy balance at the micro- and/or nano-scales required for this work is challenging, especially with temperature and power resolution in the μK and nW range, respectively.

With the advent of micromachining and microfluidic technology, high-performance microcalorimeters for chemical and biological applications were developed [1,21,22]. Systems to perform dissipated power measurements in samples with a volume in the pL range were also developed [23]. Moreover, sensitive systems are now available to measure the metabolic heat associated with different cellular processes [16,17,24,25]. The isothermal microcalorimetry was employed to detect bacteria, tumorous microtissues, and parasitic worms in a label-free manner [16]. The system was also utilized to monitor the growth of the bacteria *Pro-*

* Corresponding authors at: School of Mechanical Engineering, Northwestern Polytechnical University, Xi'an, 710072, PR China.
E-mail addresses: changhl@nwpu.edu.cn (H. Chang), pavel.neuzil@nwpu.edu.cn (P. Neužil).

https://doi.org/10.1016/j.sna.2021.112643
0924-4247/

teus mirabilis, resulting in a total energy release of ≈2.1 J with a maximum thermal power of ≈76 μW.

Recently, a microfluidic calorimeter with a sensitivity of ≈0.2 nW was reported [26]. The platform was utilized to measure the metabolic heat rate of the ciliate *Tetrahymena thermophila* and determine its spare respiratory capacity. However, the measurement platform had only one calorimeter, which could not be operated in a differential mode. The fluctuation of ambient temperature could have a non-negligible impact on the metabolic rate measurements, even within a high-vacuum environment. Moreover, the authors utilized magnetic particles to capture and immobilize the cells, which could have influenced their natural activities and, therefore, could have biased the result. A microcalorimeter to measure the metabolic heat output of *Caenorhabditis elegans* with power resolution of ≈270 pW was reported [27], allowing time-resolved measurement of a single worm from the larval to the adult stage. However, in order to perform the measurements, the specimen has to be immobilized in a capillary tube, preventing its natural movement; this has a significant impact on metabolism. Moreover, almost all the microcalorimeters developed for metabolic heat determinations have a time constant from tens to hundreds of seconds [16,26,27]. Although these heat conduction calorimeters can measure bioprocess in a dynamic manner, due to their long thermal response they are better suited for slower biological processes such as microbial growth.

Paramecium caudatum (*P. caudatum*) is a unicellular eukaryote frequent in freshwater ecosystems, widely used as a biomodel to evaluate environmental quality and the effects of xenobiotic compounds, to name the most frequent applications [28–30]. Like many other protists when under threat, *P. caudatum* activates defense mechanism by ejecting numerous sharply-pointed structures from specialized organelles called trichocysts [30]. This defense mechanism can be artificially triggered by exposing the ciliate to various surfactants e.g. Triton [31], and due to dependence on metabolic energy [31], this results in a temperature change. However, the real-time energy balance of this defense mechanism has not yet been studied.

In this work, we present a droplet-based microcalorimeter capable of dynamically monitoring the defensive behavior of *P. caudatum* with a resolution of ≈14 nW. Our differential microcalorimetric platform has a small value of thermal time constant of ≈1.5 s, therefore, it allowed the dynamic and real-time monitoring of bioprocesses in an unrestricted manner. It is important to note, that energy balance for biologists refers to the difference between energy inputs such as chemical energy from nutrients and energy outputs such as heat, motor activity, biomass chemical energy, ATP hydrolysis to ADP etc. Here we consider the system energy balance from physics point-of-view as we monitor overall energy difference inside the isolated calorimeter system.

A single protist was placed into a ≈1 μL droplet of cultivation medium, which simulated unconstrained microenvironment. We measured the temperature change of the droplet and calculated the corresponding dissipated power and consumed energy, demonstrating the potential of this approach to study chemical-induced bioprocesses of *P. caudatum*. It could be further used for analyzing other bioprocesses, such as cell division, differentiation, and apoptosis.

2. Results

2.1. Design of microcalorimetric platform and chip

We designed a microcalorimetric platform to decrease heat loss, suppress the influence of ambience, and improve sensitivity (Fig. 1a). It consists of the following three components: a thermostatic system, a microcalorimeter chip, and a microscope-based imaging system.

The thermostatic system is composed of nested outer, middle and inner chambers, which are made from brass and assembled together by plastic screws (Fig. 1b). Heaters, coolers and sensors for controlling internal temperature were fixed on the bottom of each chamber. The outer chamber and cover were connected and sealed using screws, o-rings and sealing grease. There are four connecting ports on the outer chamber: two for vacuum and pressure measurement and another two for wire connections. A view window was located on the outer cover for the observation of microcalorimeter chips and experimental phenomena. The thermostatic system provides excellent thermal isolation, which can suppress the influence of ambience.

We utilized our previously reported [32] open-chamber microcalorimeter chip designed using Nanolithography Toolbox software [33,34] to perform the metabolic heat measurements. We first deposited and patterned a sandwich layer of Cr and Au as heater and a resistance temperature detector (RTD). The RTD sensor had a spiral structure with a large sensing area of 2.4 mm^2. The absence of fluidic channels or chambers for sample injection and reaction further lowers the thermal conductance of the chip and greatly simplifies its design and fabrication (Fig. 1c). There is a close-up showing the patterned temperature sensor and heater. For details about fabrication, see Methods and Supplementary Fig. 1.

The chambers were installed on a customized microscope stage. We utilized the microscope-based imaging system to observe the cell's activity inside the droplet, using pictures and videos. The microcalorimeter chip and printed circuit board (PCB) were assembled in the inner chamber.

The surface of fabricated microcalorimeter chips was coated with fluorosilane [35] and two chips were directly soldered to the customized PCB (Fig. 1d). With two external resistors, we formed a Wheatstone bridge in a differential configuration to reject the common mode. We only measured the differences between resistances of two RTDs, thereby suppressing the influence of ambience and improving the sensitivity. However, evaporation of water from sample droplets would cause heat loss and a change in thermal capacitance, leading to increased error in the measurement. Therefore, we covered the sample with mineral oil, forming a virtual reaction chamber (VRC) (Fig. 1d). The VRC prevented the evaporation of samples, thus eliminating the related heat loss. Mineral oil of high purity grade is traditionally used to prevent biological systems against evaporation [36]. Also the VRC and sensor/heater were separated from each other by the glass substrate preventing the liquids from influencing the properties of the sensors. Moreover, we did not observe any degradation of the hydrophobic coating on the surface of microcalorimeter chips.

2.2. Characterization of microcalorimeter

The principle of calorimetric measurement can be described as follows: first, the metabolic heat output generated by a biosample will cause a temperature change (ΔT) in the droplet; then the ΔT will be detected by the sensor (RTD) on the microcalorimeter chip, with the heat output calculated by using the heat balance equation:

$$C\frac{d\Delta T}{dt} + G \cdot \Delta T = P \quad (1)$$

where C, t, G and P are thermal capacitance, time, thermal conductance of the chip, and dissipated power, respectively. Before measuring the metabolic heat of the bioprocesses, we characterized the thermal properties of the microcalorimeter chip by methods described earlier [32], including electrical resistance (R) and

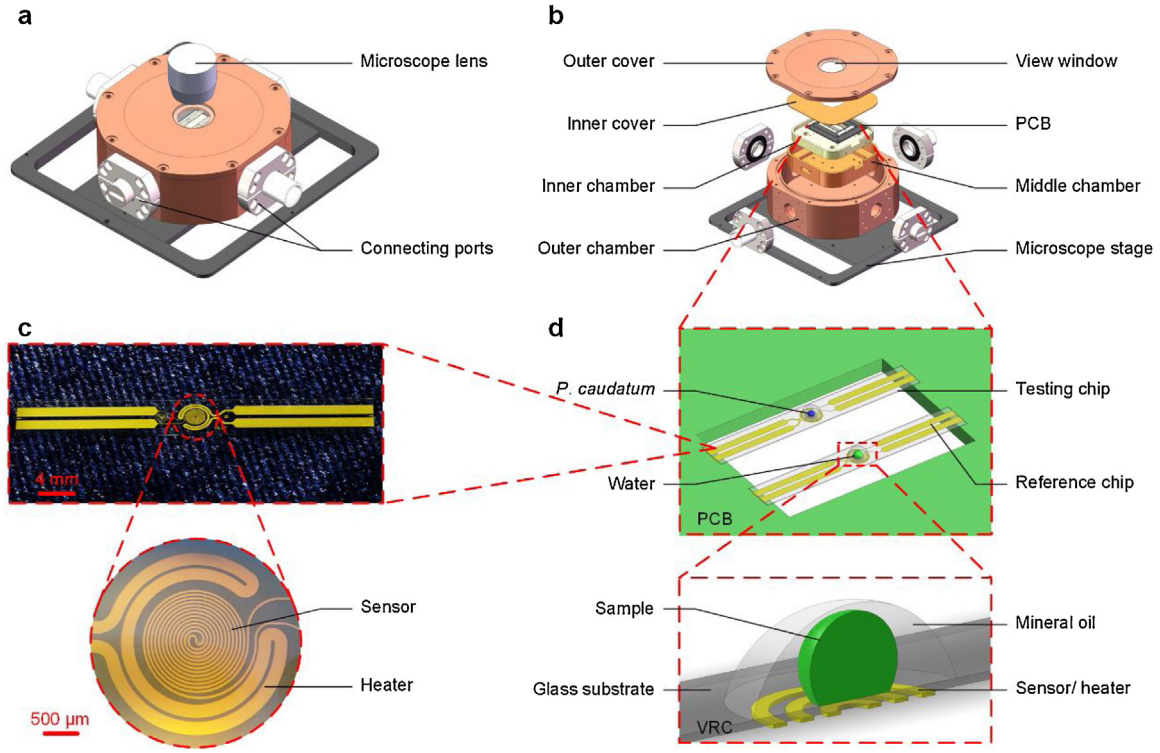

Fig. 1. Design of microcalorimetric platform and chip. (**a**) The assembled microcalorimetric platform containing thermostatic system, microscope-based imaging system and microcalorimeter chip. The connecting ports are used for vacuum and pressure measurement, as well as for wire connections. (**b**) The explosive view of the platform. The thermostatic system consisting of three nested isolation chambers is used for optimal thermal isolation, which can suppress the influence of ambience. Each chamber has its own heater, cooler and sensor for internal temperature controlling. A view window is located on the outer cover for the observation of experimental phenomena. The PCB with microcalorimeter chips is assembled into an inner chamber. (**c**) The fabricated microcalorimeter chip and a close-up of sensor and heater both made of Au. The sensor has a spiral structure and is surrounded by the heater. (**d**) The setup of PCB with microcalorimeter chips and a close-up of the virtual reaction chamber (VRC). Two chips are soldered onto PCB, forming a differential configuration to reject the common mode. The samples are dispensed into a droplet of mineral oil, forming a VRC to prevent the evaporation. The VRC and sensor/heater are separated by the glass substrate, so there is no influence between them.

temperature coefficient of resistance (α) of the sensor, thermal conductance, capacitance and time constant (τ) of the chip, and the thermal resolution and sensitivity of the microcalorimeter.

We measured the R and α of the sensor on the microcalorimeter chip using the four-point probe method (see Methods and Supplementary Fig. 2). We obtained the resistance at 0 °C (R_0) and α as (109.7 ± 0.2) Ω and (3.15 ± 0.07) × $10^{-3}K^{-1}$, respectively - both (mean ± standard deviation). The RTD was then connected to a Wheatstone bridge (Fig. 2a) [37]. R_1, R_S and R_F represent the variable resistor for adjusting the balance of the bridge, the resistance of RTD and the fixed resistors with nominal resistance of 1 kΩ, respectively. The Wheatstone bridge was powered by a sinus-shaped voltage with an V_B amplitude of 100 mV root mean square (RMS) provided by a lock-in amplifier internal power supply. The Wheatstone bridge output voltages were subtracted from each other and amplified by an internal differential amplifier with gain (G_D) set to 991, then processed by a voltage preamplifier with gain (G_V) of 1, and, finally, by a lock-in amplifier with sensitivity set to 100 mV. The lock-in amplifier output voltage (ΔV_L) was recorded by an oscilloscope. The temperature response (T_T) of the microcalorimeter can be derived as follows:

$$T_T = \frac{\Delta V_L}{\Delta T} = 10\frac{\alpha \cdot V_B \cdot G_D \cdot G_V}{4 \cdot S} \quad (2)$$

We calculated the temperature response of ≈7.8 $V{\cdot}K^{-1}$; then, the voltage output was converted to the temperature signal using $\Delta T = \Delta V/T_T$, and the voltage input was converted to power input using $P = V_B^2/(4{\cdot}R_S)$ (Fig. 2b). Therefore, the thermal conductance can be calculated using Eq. (1) in steady state: $G = P/\Delta T$ ≈282.3 $\mu W{\cdot}K^{-1}$. The time constant was extracted as τ = 1.5 s, a very low value allowing us to measure fast biological processes. Then the thermal capacitance C was calculated as $G{\cdot}\tau$ ≈423.5 $\mu J{\cdot}K^{-1}$.

We evaluated the sensitivity of the microcalorimeter by determining the system noise with set V_B of 100 mV RMS, G_D = 991, G_V = 20, and S =1 mV, providing a T_T value of ≈1561 $V{\cdot}K^{-1}$, according to Eq. (2). We then calculated the temperature noise (T_{noise}) as ≈49.7 μK (Fig. 2c). As a result, the sensitivity of our microcalorimeter was calculated as $P_s = G{\cdot}T_{noise}$ ≈14 nW. Although the sensitivity of our calorimeter did not supersede two recently reported works [26,27], our microcalorimeter is still one of the best metabolic heat measurement platforms reported until now. There is still a room for improvement by lowering the G value of the glass substrate as well as improve thermal stability of the chamber, which will be addressed in our next-generation microcalorimeter.

We also estimated the self-heating of RTD during the measurements. The applied voltage V_B has an amplitude of 100 mV RMS to keep the temperature increase (ΔT_{SH}) of the microcalorimeter chip due to the self-heating effect minimized as:

$$\Delta T_{SH} = \frac{V_B^2}{4 \cdot G \cdot R_0} \quad (3)$$

The ΔT_{SH} was calculated as ≈80.7 mK, causing a fixed offset at the bridge output, since the V_B is applied during entire measurements. This offset is further eliminated by the bridge configuration in a fully differential mode as shown before [37], therefore, it does not influence the metabolic heat measurements.

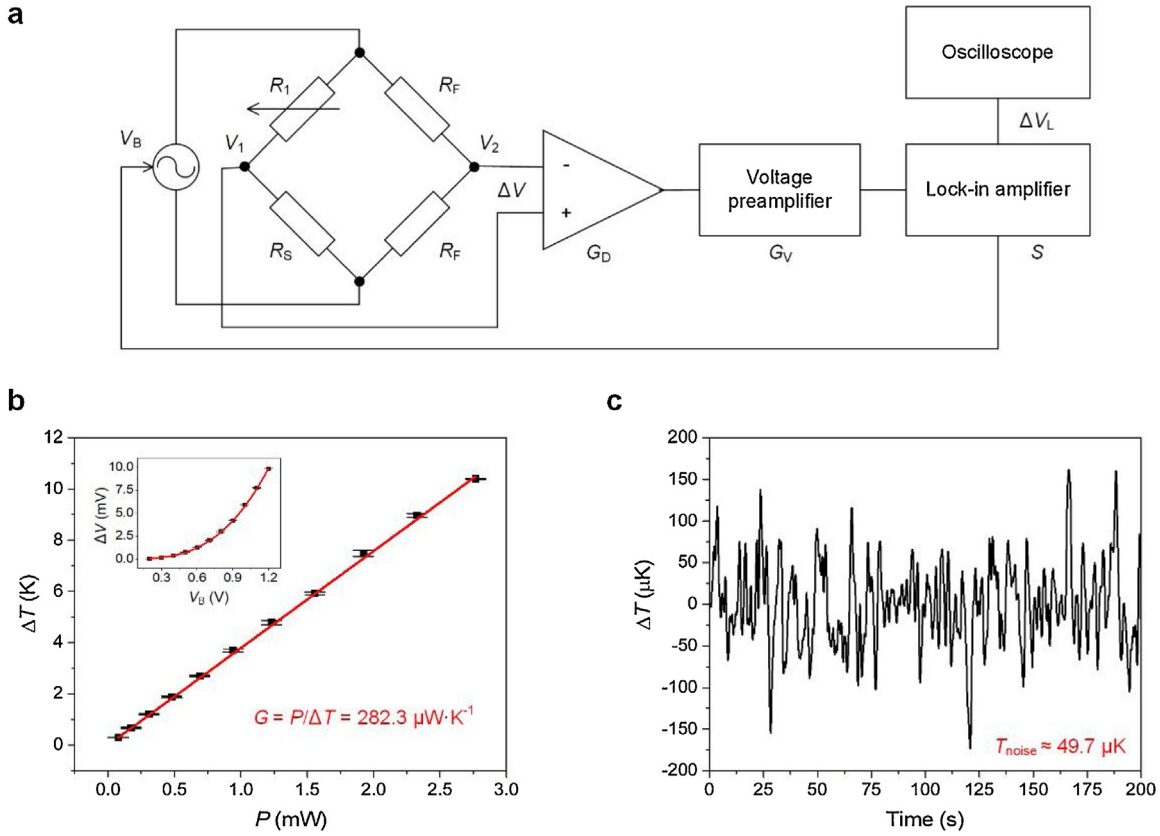

Fig. 2. Characterization of microcalorimeter. (**a**) The schematic of electric circuit for microcalorimeter chip characterization. The chip is connected into a Wheatstone bridge, as R_S. R_1 and R_F are the variable and fixed resistors. The bridge is powered by a lock-in amplifier and its output is then processed by a differential amplifier, a voltage preamplifier, and a lock-in amplifier, and is finally recorded by an oscilloscope. (**b**) The ΔT according to the applied power. The thermal conductance can be calculated using $G = P/\Delta T \approx 282.3$ μW·K^{-1}. (**c**) The noise measurement. The temperature fluctuation of the system is measured by an RTD for ≈200 s. The RMS temperature noise is ≈49.7 μK; therefore, the sensitivity of our microcalorimeter was ≈14 nW. Source data for 2**b** and 2**c** are provided as Source Data files.

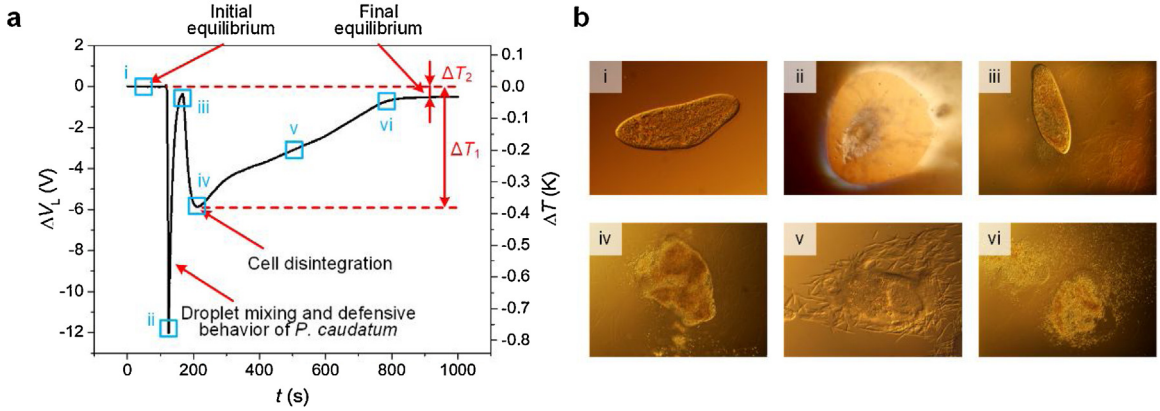

Fig. 3. Real-time monitoring of the defensive behavior of *P. caudatum*. (a) The voltage output (ΔV_L) as a function of t in monitoring the defensive behavior. The result shows the different stages of measurements, including droplet dispensing and mixing, the defensive behavior of *P. caudatum*, and its disintegration. The first peak is caused by droplet mixing and defensive behavior, while the second one is induced by cell disintegration. The temperature difference ΔT_1 represents the Triton-induced death and cell disintegration, with the difference between initial and final equilibrium ΔT_2 being the normal metabolism of *P. caudatum*. (**b**) The photos capturing different stages corresponding to the blue boxes in Fig. 3a. (i) *P. caudatum* with an intact membrane; (ii) the blast-like defensive behavior; (iii) trichocyst arrows scattered nearby and a broken membrane with leakage of cellular material at left bottom; (iv) dissolving membrane; (v) ruptured membrane, likely a consequence of an uncontrolled massive release of trichocysts arrows; (vi) cellular debris. Source data for 3**a** is provided as a Source Data file. (For interpretation of the references to colour in this figure legend, the reader is referred to the web version of this article).

2.3. *Real-time monitoring of the defensive behavior of* P. caudatum

We utilized our nanowatt droplet-based differential microcalorimetric platform to monitor the energy balance and measure the corresponding dissipation and energy change of the defensive behavior of *P. caudatum* induced by the addition of Triton X-100 (Triton) The experiments were conducted using two microcalorimeter chips connected to a Wheatstone bridge in a fully differential mode (Fig. 1d; Supplementary Fig. 3). The detection circuit is modified from Fig. 2a by replacing the two fixed resistors (R_F) with an adjustable resistor (R_2) and a reference resistor (R_R).

The differential system significantly suppresses ambient noise and improves the accuracy of metabolic heat measurements. The Wheatstone bridge was powered with an amplitude of V_B set to 100 mV RMS, and the output ΔV_L was recorded with an oscilloscope and converted into ΔT using Eq. (2) (Fig. 3a).

We placed a ≈0.5 μL droplet of suspension containing *P. caudatum* on the testing microcalorimeter chip and a ≈1 μL droplet of water on the reference chip. Both droplets were subsequently covered with ≈4.0 μL of mineral oil, forming the VRC to suppress the water evaporation.

The platform was aligned using a microscope and the counted number of *P. caudatum* was five. The system was first initialized to equilibrium from t ≈0 s. At that moment, due to the sufficient living space and nutrients, *P. caudatum* behaved naturally and had an intact membrane (Fig. 3b i). We then added a ≈0.5 μL Triton droplet into the VRC on the testing chip at t ≈115 s. The two droplets mixed inside the VRC, and when the protist came into contact with Triton, it quickly moved away and activated its defense mechanism by ejecting numerous sharply-pointed arrows from organelles called trichocysts, which are localized under its cellular membrane. This activity is very fast, corresponding to a time range between ≈133 ms and ≈165 ms (see supplementary Video), which is in a similar time frame to previously reported values [30].

Meanwhile, a phenomenon looking like *exploding of a bomb* was observed, creating a clear area (Fig. 3b ii). The droplets mixing and the defensive behavior consumed energy and caused a temperature decrease by ≈750 mK at t ≈125 s. The microcalorimeter temperature then gradually increased and reached almost the equilibrium value of ≈23 mK at t ≈168 s. There was a *P. caudatum* with *arrows* scattered nearby, with leakage of cellular material at the left bottom part of the cell (Fig. 3b iii), while the cell membrane still looked intact.

After that, the temperature decreased again and reached the second peak at t ≈211 s. During this time, we observed the disintegration of *P. caudatum* membrane (Fig. 3b iv). This is because Triton destroys the membrane structure and increases its permeability. The membrane disintegration consumed energy, causing a ΔT of ≈365 mK, and the *P. caudatum* gradually lost its viability. The cellular material was released massively (Fig. 3b v), increasing ΔV_L. Finally, the *P. caudatum* membrane was completely dissolved, releasing the cellular contents (Fig. 3b vi), and the system gradually reached the final equilibrium of ≈33 mK at t ≈900 s. We recorded a video using a CMOS camera with a 20.2-megapixel imager and 30 frames·s^{-1}, showing the defensive behavior of *P. caudatum* upon the addition of Triton (see supplementary video).

Energetic processes in cells are complex and catabolic exothermic reactions are tightly coupled with endothermic anabolic processes and the process of exocytosis is no exception. Since the trichocyst exocytosis is an endothermic process [38,39], this mechanisms of cell defense requires an energy. The endothermic phase of exocytosis could be observed from phase i to phase ii (Fig. 3a). Then there is system relaxation bringing the microcalorimeter back to original temperature (ii to iii) and the metabolisms of cells returns nearly to the original state (ii-iii). In this phase the cell membrane is probably reconstructed after its massive fusion with trichocysts in the previous phase [40]. This is supported by our observation using microscope where the cell till phase iii seemed to be intact. The second decrease of the signal (iii-iv) could be assigned to the lysis of cells due to the persistent presence of toxic concentrations of Triton in the medium. *P. caudatum* is equipped with contractile vacuole which ensures the broad range of its osmotic resistance [41] but the detergent Triton in the concentration needed for exocytosis stimulation and after longer exposition destroys physiological functions of cell membrane. We observed its rupture, cell lysis and slow first temperature decrease and later on increase back to original equilibrium (Fig. 3a iv-vi).

Besides the key experiment described above, we also performed a set of reference experiments always using volume of ≈0.5 μL of a hay extract solution having typically one of two *P. caudatum* covered with ≈4 μL of mineral oil. Then we added different solutions (see below) with volume of ≈0.5 μL to merge with a fresh hay extract with one or two *P. caudatum*, such as DI water, hay extract, DI water with ≈0.001 % of Triton solution (experiment described above in Fig. 3), DI water with ≈0.0005 % of Triton solution, DI water with ≈0.00025 % of Triton solution, and DI water with ≈0.0001 % of Triton solution.

Only samples containing stronger contents of Triton had an effect on the *P. caudatum*. Adding ≈0.001 % of Triton immediately killed *P. caudatum*. Adding ≈0.0005 % Triton solution killed *P. caudatum* in a few s while ≈0.0001 % Triton solution did not exhibit any obvious effect on *P. caudatum*. We can therefore conclude that it is the Triton and not osmotic effect destroying *P. caudatum,* which is in an agreement with previously published work showing *P. caudatum* having specialized organelle (the contractile vacuole) with an ability to regulate osmotic pressure [41]. Presence of this organelle allows survival of *P. caudatum* in solutions with different content of ions therefore we did not observe the different behavior of cells in DI water and hay extract.

From the real-time monitoring measurements, we can draw the conclusion that three activities are responsible for ΔT: first, droplet dispensing and mixing, which cause a temperature decrease; then, the blast-like defensive behavior of *P. caudatum*, which brings a quick and dramatic temperature drop; finally, the disintegration of cell membrane, which induces a continuous and moderate temperature decrease. We analyzed and calculated ΔT, dissipated power (ΔP) and consumed energy (E) corresponding to each of these activities (Fig. 4).

We transformed the ΔV_L amplitude in the range from t ≈100 s to t ≈168 s (Fig. 4a) into ΔT and ΔP (Fig. 4b) using Eqs. (1) and (2) by a MATLAB script (see Supplementary Information). We found that there were two peaks from t ≈120 s to t ≈127 s, matching with the two activities of droplet mixing and defensive behavior. The first peak was induced by droplet mixing, with a value of ≈501 μW at t ≈121.4 s, while the second one resulted from the blast-like defensive behavior, with a value of ≈1476.6 μW at t ≈123.7 s. To verify the above conjectures, we performed control experiments where Triton was added into a droplet without *P. caudatum*, which means solution mixing in the absence of any bioprocess. We monitored the ΔV_L signal (Fig. 4c) and converted it to ΔT and ΔP (Fig. 4d). The results showed only one drop, caused by droplets mixing, and then the curves reached the final equilibrium. Therefore, we conclude that the second peak or peaks of ΔP were caused by the defensive behavior of *P. caudatum*. The E was calculated by performing a curve fitting using the Levenberg-Marquardt method in the range from ≈123 s to ≈126 s by the Lorentz function (green curve in Fig. 4b):

$$P = P_0 + \frac{2E}{\pi} \cdot \frac{w}{4(t - t_0)^2 + w^2}, \tag{4}$$

where P_0 is a power offset set to 0 W, and then determining the area under the Lorentz function representing total consumed energy during the defensive behavior. The t_0 is the peak location, and w is the function width. The E value was determined to be (2.52 ± 0.04) mJ (mean ± fitting error), and since there were five *P. caudatum* cells present in the droplet, the mean values of ΔP and E associated with a single-cell defense mechanism were ≈295.3 μW and ≈0.50 mJ, respectively. As previously discussed, when analyzing the video, the ejection of trichocysts from individual cells—i.e. the defensive behavior—is an asynchronous process triggered at different times in individual cells. In a few experiments, this process was delayed in one or two cells, and there was a peak related to a single event (Fig. 4e and f). We calculated the E value of each

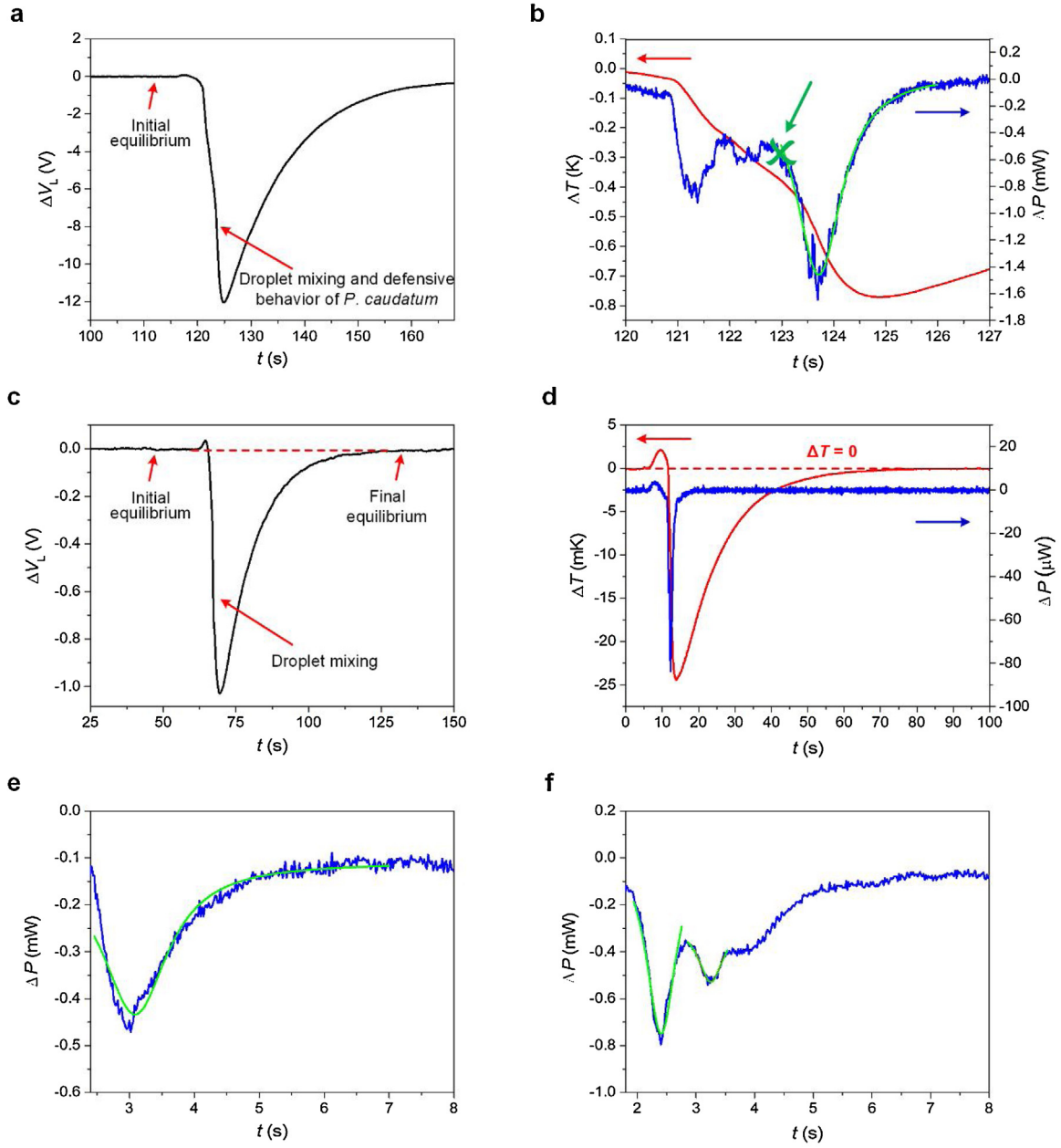

Fig. 4. Measurements of real-time energy balance monitoring the defensive behavior. (**a**) The voltage output (ΔV_L) of defensive behavior monitoring as a function of t from ≈100 s to ≈168 s. The peak represents the addition of Triton, triggering the defense mechanism. (**b**) ΔT and ΔP as a function of t in range from t ≈120 s to t ≈127 s, converted from ΔV_L in Fig. 4a using Eqs. (1) and (2). The green curve fitting represents the consumed energy. The green cross and arrow represent the beginning of the defensive behavior, corresponding to ≈9 min 5 s in the attached video. (**c**) The voltage output in the control experiment. Only one peak occurs, representing the droplets mixing. (**d**) The ΔT and ΔP as a function of t in the control experiment. There is no output change between the initial and final equilibrium. (**e**) The ΔP and its curve fitting related to one *P. caudatum* defense mechanism. (**f**) The ΔP related to two defensive events. The red, blue and green lines represent ΔT, ΔP, and the fitting curves using the Lorentz function, respectively. All these data are available in Source Data files. (For interpretation of the references to colour in this figure legend, the reader is referred to the web version of this article).

event, resulting in a value of (0.73 ± 0.08) mJ (mean ± standard deviation).

At t ≈168 s, *P. caudatum* started to disintegrate and release its cellular content. As described above, this process resulted in a continuous and moderate temperature decrease. At t ≈211 s, it reached a peak with a value of ΔT_1 ≈376 mK, after which the cell membranes were gradually lysed (disintegrated). The system reached the final equilibrium at t ≈900 s, with a ΔT_2 of ≈33 mK compared with the initial equilibrium (Fig. 3a). The final equilibrium is equal to the initial equilibrium in the control experiments (ΔT =0 K) (Fig. 4c and d). Vital *P. caudatum* has an active metabolism, resulting in dissipating heat—which was, of course, not taking place at the end of the experiments. Therefore, due to the termination of *P. caudatum*'s metabolism, the final T is lower than the T at the beginning of the experiments with live ciliates. Here, we defined ΔT_1 as the ΔT of Triton-induced death and ΔT_2 as the ΔT of active metabolism. We calculated the ΔT and ΔP values caused by a single cell in the steady state, resulting in ΔT_1 and P_1 of ≈75.2 mK and ≈21.2 μW and ΔT_2 and P_2 of ≈6.6 mK and ≈1.9 μW, respectively.

We repeated the energy balance monitoring experiments several times (n = 16) and calculated the average ΔT and ΔP of *P. caudatum*. The average ΔT_1 and ΔP_1 of Triton-induced death were

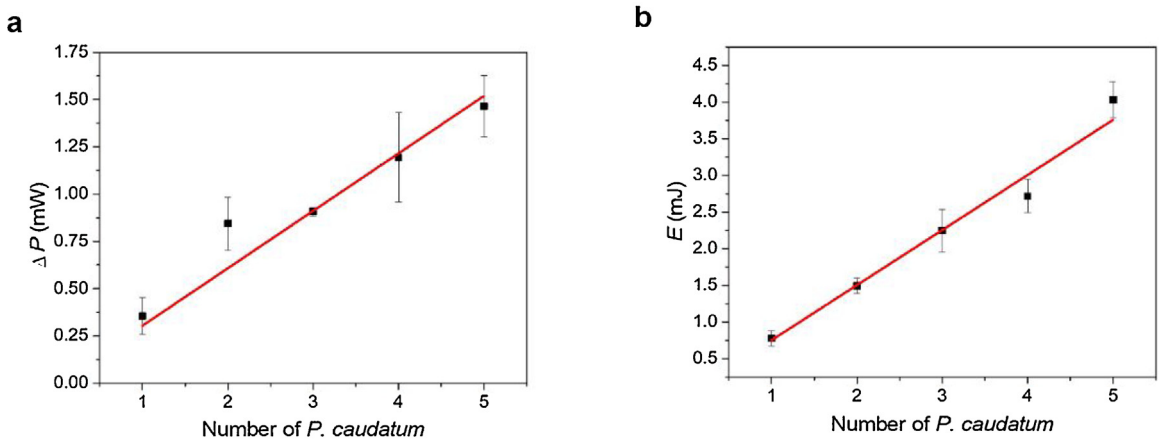

Fig. 5. Experimental results of ΔP and E of defensive behavior (**n = 16**). (**a**) The ΔP and (**b**) E values obtained with different number of *P. caudatum* cells. All these data are available in Source Data files.

(78.0 ± 1.3) mK and (22.0 ± 0.4) μW, while the average ΔT_2 and ΔP_2 of its metabolism were (6.6 ± 0.15) mK and (1.9 ± 0.04) μW, respectively. In the meantime, we measured ΔP and E of defensive behavior with different numbers of cells (Fig. 5a and b). The mean values of ΔP and E associated with a single-cell defense mechanism were (303.8 ± 6.3) μW and (0.75 ± 0.02) mJ, respectively. These results are in good agreement with the ones from single events calculated above using data from Fig. 4e and f.

3. Discussion

We measured the metabolic processes of *P. caudatum* including Triton-induced defensive behavior followed by cell lysis using a droplet-based differential microcalorimetric platform by monitoring its temperature change. Then we used heat balance equation to determine the dissipated power corresponding to the measured temperature change. The results including temperature change, dissipated power, and consumed energy were analyzed to evaluate the defensive behavior by the ejection of trichocysts. We were able to show that our nW droplet-based differential microcalorimeter system has sufficient sensitivity to analyze thermodynamics of these processes and their mechanisms. Although our platform is not the most sensitive system when compared with other studies [26,27], it can monitor and measure the energy balance of bioprocesses in a noninvasive and non-immobilized manner, which could lead to more real and reliable results than other labeled and immobilized methods. However, the sensitivities reported so far are still not sufficient for monitoring the thermodynamics of living mammalian cells [38,42]. We are pursuing this goal by decreasing the sample volume in order to obtain faster response with better temperature sensitivity.

In summary, we showed a simple yet fast and sensitive microcalorimetry system for monitoring the real-time energy balance of a unicellular eukaryote by using a nW droplet-based differential microcalorimeter with a temperature and power resolution of ≈49.7 μK and ≈14 nW, respectively. The microcalorimeter has a short response time of ≈1.5 s, and thus allowed the dynamic and real-time monitoring of fast bioprocesses. We selected the defense mechanism of the protist *P. caudatum* because it is the fastest known synchronous exocytosis. We monitored the energy balance due to the activation of the trichocyst exocytosis upon its induction by Triton. We found this process is endothermic, which is in line with previously published work [31].

We calculated the mean values of dissipated power and consumed energy corresponding to a single cell exocytosis event of ≈303.8 μW and ≈0.75 mJ, respectively. Meanwhile, the average temperature change and dissipated power from a single *P. caudatum* metabolism were established as ≈6.6 mK and ≈1.9 μW, while the average values of Triton-induced exocytosis followed by cell death were ≈78.0 mK and ≈22.0 μW, respectively.

Our measurements demonstrated that the nanowatt droplet-based microcalorimeter is capable of dynamically measuring the energy balance of bioprocesses in microorganisms in a non-invasive and non-immobilized way. Furthermore, it can be expanded to study other biological processes, such as the formation of the neutrophil extracellular traps during netosis, when neutrophils eject primarily their genomic DNA to form nets to catch infectious agents [43]. Such further studies would epitomize how many intriguing phenomena can be investigated when we adapt and improve our knowledge by integrating physics with life science.

4. Methods

4.1. Microcalorimeter chip fabrication

The microcalorimeter chips were fabricated on a glass substrate, with diameter and thickness of ≈100 mm and ≈100 μm, respectively. As shown in Supplementary Fig. 1, we deposited Cr/Au with thickness of ≈10 nm and ≈100 nm, respectively. Next, we transferred the chip pattern onto the substrate using ultraviolet lithography with positive photoresist (PR), followed by a metal sandwich etching using KI/I_2-based Au etchant and $(NH_4)_2[Ce(NO_3)_6]$-based Cr etchant solution. We then diced the wafer into individual chips with a size of (4 × 30) mm^2 using a diamond dicing saw. The final steps were the PR removal and the cleaning of the chips.

4.2. Determination of resistance (R_0) and temperature coefficient of resistance (α) of the sensor

The R_0 and α of the sensor on the microcalorimeter chip were measured using the four-point probe method. We placed the microcalorimeter chip on a hotplate and measured its R value as functions of ΔT. The hotplate temperature was monitored by a Pt100 temperature sensor from ≈20 °C to ≈50 °C, with a temperature increase of ≈5 °C between two measurements. Finally, we performed a linear fitting of the measured data using formula $R = R_0(1 + \alpha\Delta T)$ and calculated the R_0 and α. Two examples are shown in Supplementary Fig. 2.

4.3. *Preparation of* P. caudatum *and all chemicals*

The culture medium was prepared by being infused with hay overnight in deionized water, spun, and autoclaved. The *P. caudatum* was cultured in hay extract and prepared to a content of $\approx 8 \times 10^3$ cells·mL^{-1}. The Triton X-100 was diluted with deionized water to a content of ≈0.001 %. All chemicals were prepared with deionized water produced in-house, which has a specific resistivity greater than 18.0 MΩ·cm at 25 °C.

Data availability

Source data for Figs. 2b, c, 3 a, 4 a–f, 5 a, and b and Supplementary Fig. 2a and b are available in Source Data files. All other data supporting the findings of this study are available from the corresponding author upon reasonable request.

CRediT authorship contribution statement

Jianguo Feng: Writing - original draft, Methodology. **Hanliang Zhu:** Data curation, Investigation. **Julius Lukeš:** Investigation. **Marie Korabečná:** Investigation. **Zdenka Fohlerová:** Resources, Investigation. **Ting Mei:** Software. **Honglong Chang:** Supervision. **Pavel Neužil:** Conceptualization, Writing - review & editing.

Declaration of Competing Interest

The authors declare that they have no known competing financial interests or personal relationships that could have appeared to influence the work reported in this paper.

Acknowledgements

This work was supported by a W099109 grant from P.R China. The work was also supported by the Grant Agency of the Czech Republic (17-20716S) and the Ministry of Education, Youth and Sports of the Czech Republic under the project OP VVV CEITEC Nano+ (CZ.02.1.01/0.0/0.0/16_013/0001728). MK was supported by Grants LTACH19005 and Progress Q25/LF1 of the Ministry of Education, Youth and Sport of the Czech Republic, and by Grant RVO-VFN 64165 of the Ministry of Health of the Czech Republic. JL was supported by the ERD project OP VVV 16_019/0000759 and ERC CZ LL1601.

Appendix A. Supplementary data

Supplementary material related to this article can be found, in the online version, at doi:https://doi.org/10.1016/j.sna.2021.112643.

References

[1] S. Wang, S. Yu, M. Siedler, P.M. Ihnat, D.I. Filoti, M. Lu, et al., A power compensated differential scanning calorimeter for protein stability characterization, Sens. Actuators B Chem. 256 (2018) 946–952.
[2] B. Wang, Y. Jia, Q. Lin, A microfabrication-based approach to quantitative isothermal titration calorimetry, Biosens. Bioelectron. 78 (2016) 438–446.
[3] O. Braissant, D. Wirz, B. Göpfert, A.U. Daniels, Use of isothermal microcalorimetry to monitor microbial activities, FEMS Microbiol. Lett. 303 (2010) 1–8.
[4] O. Braissant, A. Bachmann, G. Bonkat, Microcalorimetric assays for measuring cell growth and metabolic activity: methodology and applications, Methods 76 (2015) 27–34.
[5] O. Braissant, M. Astasov-Frauenhoffer, T. Waltimo, G. Bonkat, A review of methods to determine viability, vitality, and metabolic rates in microbiology, Front. Microbiol. 11 (2020).
[6] K.Y. Tan, C.Y. Li, Y.F. Li, J.J. Fei, B. Yang, Y.J. Fu, et al., Real-time monitoring ATP in mitochondrion of living cells: a specific fluorescent probe for ATP by dual recognition sites, Anal. Chem. 89 (2017) 1749–1756.
[7] T. Maskow, R. Kemp, F. Buchholz, T. Schubert, B. Kiesel, H. Harms, What heat is telling us about microbial conversions in nature and technology: from chip-to megacalorimetry, Microb. Biotechnol. 3 (2010) 269–284.
[8] A. Majumdar, Scanning thermal microscopy, Annu. Rev. Mater. Sci. 29 (1999) 505–585.
[9] K. Okabe, N. Inada, C. Gota, Y. Harada, T. Funatsu, S. Uchiyama, Intracellular temperature mapping with a fluorescent polymeric thermometer and fluorescence lifetime imaging microscopy, Nat. Commun. 3 (2012) 705.
[10] J.S. Donner, S.A. Thompson, M.P. Kreuzer, G. Baffou, R. Quidant, Mapping intracellular temperature using green fluorescent protein, Nano Lett. 12 (2012) 2107–2111.
[11] Y. Cui, R. Liu, F. Ye, S. Zhao, Single-excitation, dual-emission biomass quantum dots: preparation and application for ratiometric fluorescence imaging of coenzyme A in living cells, Nanoscale 11 (2019) 9270–9275.
[12] G. Glotz, D.J. Knoechel, P. Podmore, H. Gruber-Woelfler, C.O. Kappe, Reaction calorimetry in microreactor environments-measuring heat of reaction by isothermal heat flux calorimetry, Org. Process Res. Dev. 21 (2017) 763–770.
[13] L. Zuo, X. Chen, S. Yu, M. Lu, Design and fabrication of a differential scanning nanocalorimeter, J. Micromech. Microeng. 27 (2017), 025006.
[14] P. Zheng, Y. Ma, X. Peng, T. Yin, X. An, W. Shen, Determination of the interaction enthalpy between microemulsion droplets by isothermal titration microcalorimetry, Langmuir 27 (2011) 12280–12283.
[15] T. Maskow, T. Schubert, A. Wolf, F. Buchholz, L. Regestein, J. Buechs, et al., Potentials and limitations of miniaturized calorimeters for bioprocess monitoring, Appl. Microbiol. Biotechnol. 92 (2011) 55–66.
[16] O. Braissant, J. Keiser, I. Meister, A. Bachmann, D. Wirz, B. Gopfert, et al., Isothermal microcalorimetry accurately detects bacteria, tumorous microtissues, and parasitic worms in a label-free well-plate assay, Biotechnol. J. 10 (2015) 460–468.
[17] O. Borens, E. Yusuf, J. Steinrücken, A. Trampuz, Accurate and early diagnosis of orthopedic device-related infection by microbial heat production and sonication, J. Orthop. Res. 31 (2013) 1700–1703.
[18] J. Lerchner, K. David, F. Unger, K. Lemke, T. Förster, F. Mertens, Continuous monitoring of drug effects on complex biological samples by segmented flow chip calorimetry, J. Therm. Anal. Calorim. 127 (2017) 1307–1317.
[19] M. Gysin, O. Braissant, K. Gillingwater, R. Brun, P. Mäser, T. Wenzler, Isothermal microcalorimetry – a quantitative method to monitor Trypanosoma congolense growth and growth inhibition by trypanocidal drugs in real time, Int. J. Parasitol. Drugs Drug Resist. 8 (2018) 159–164.
[20] T. Wenzler, A. Steinhuber, S. Wittlin, C. Scheurer, R. Brun, A. Trampuz, Isothermal microcalorimetry, a new tool to monitor drug action against Trypanosoma brucei and Plasmodium falciparum, PLoS Negl. Trop. Dis. 6 (2012) e1668.
[21] W. Lee, W. Fon, B.W. Axelrod, M.L. Roukes, High-sensitivity microfluidic calorimeters for biological and chemical applications, Proc. Natl. Acad. Sci. U. S. A. 106 (2009) 15225–15230.
[22] M.M. Huie, D.C. Bock, A.M. Bruck, K.R. Tallman, L.M. Housel, L. Wang, et al., Isothermal microcalorimetry: insight into the impact of crystallite size and agglomeration on the lithiation of magnetite, Fe_3O_4, ACS Appl. Mater. Interfaces 11 (2019) 7074–7086.
[23] S. Ni, H. Zhu, P. Neuzil, L. Yobas, JMEMS letters a SiN microcalorimeter and a non-contact precision method of temperature calibration, J. Microelectromech. Syst. 29 (5) (2020) 1103–1105.
[24] L. Wernli, G. Bonkat, T.C. Gasser, A. Bachmann, O. Braissant, Use of isothermal microcalorimetry to quantify the influence of glucose and antifungals on the growth of Candida albicans in urine, J. Appl. Microbiol. 115 (2013) 1186–1193.
[25] T. Hartmann, N. Barros, A. Wolf, C. Siewert, P.L.O. Volpe, J. Schemberg, et al., Thermopile chip based calorimeter for the study of aggregated biological samples in segmented flow, Sens. Actuators B Chem. 201 (2014) 460–468.
[26] S. Hong, E. Dechaumphai, C.R. Green, R. Lal, A.N. Murphy, C.M. Metallo, et al., Sub-nanowatt microfluidic single-cell calorimetry, Nat. Commun. 11 (2020), 2982.
[27] S. Hur, R. Mittapally, S. Yadlapalli, P. Reddy, E. Meyhofer, Sub-nanowatt resolution direct calorimetry for probing real-time metabolic activity of individual C. elegans worms, Nat. Commun. 11 (2020), 2983.
[28] M. Delmonte Corrado, A. Amaroli, F. Trielli, C. Falugi, Cholinesterase enzyme activity in protists and environmental biomonitoring, Trends Microbiol. 2 (2006) 123–136.
[29] H. Benbouzid, H. Berrebbah, M. Berredjem, M.-R. Djebar, Toxic effects of phosphoramidate on Paramecium sp. with special emphasis on respiratory metabolism, growth, and generation time, Toxicol. Environ. Chem. 94 (2012) 557–565.
[30] H. Plattner, Trichocysts - Paramecium's projectile-like secretory organelles: reappraisal of their biogenesis, composition, intracellular transport, and possible functions, J. Eukaryot. Microbiol. 64 (2017) 106–133.
[31] H. Matt, M. Bilinski, H. Plattner, Adenosinetriphosphate, calcium and temperature requirements for the final steps of exocytosis in Paramecium cells, J. Cell. Sci. 32 (1978) 67–86.
[32] J. Feng, P. Podesva, H. Zhu, J. Pekarek, C.C. Mayorga-Martinez, H. Chang, et al., Droplet-based differential microcalorimeter for real-time energy balance monitoring, Sens. Actuators B Chem. (2020), 127967.
[33] K.C. Balram, D.A. Westly, M. Davanco, K.E. Grutter, Q. Li, T. Michels, et al., The nanolithography toolbox, J. Res. Inst. Stand. Technol. 121 (2016) 464–475.
[34] H. Zhang, J. Pekárek, J. Feng, X. Liu, H. Li, H. Zhu, et al., Nanolithography toolbox—simplifying the design complexity of microfluidic chips, J. Vac. Sci.

Technol. B Nanotechnol. Microelectron. Mater. Process. Meas. Phenom. 38 (2020), 063002.
[35] E.R. Castro, M.D. Tarn, P. Ginterová, H. Zhu, Y. Xu, P. Neužil, Determination of dynamic contact angles within microfluidic devices, Microfluid Nanofluid 22 (2018) 51.
[36] E.A. Johannessen, J.M. Weaver, L. Bourova, P. Svoboda, P.H. Cobbold, J.M. Cooper, Micromachined nanocalorimetric sensor for ultra-low-volume cell-based assays, Anal. Chem. 74 (2002) 2190–2197.
[37] V. Svatoš, I. Gablech, J. Pekárek, J. Klempa, P. Neužil, Precise determination of thermal parameters of a microbolometer, Infrared Phys. Technol. 93 (2018) 286–290.
[38] G.B. West, W.H. Woodruff, J.H. Brown, Allometric scaling of metabolic rate from molecules and mitochondria to cells and mammals, Proc. Natl. Acad. Sci. U. S. A. 99 (2002) 2473–2478.
[39] J. Padawer, Exocytosis, in: P.J. Delves (Ed.), Encyclopedia of Immunology, second edition, Elsevier, Oxford, 1998, pp. 849–856.
[40] J. Vilmart-Seuwen, H. Kersken, R. Stürzl, H. Plattner, ATP keeps exocytosis sites in a primed state but is not required for membrane fusion: an analysis with Paramecium cells in vivo and in vitro, J. Cell Biol. 103 (1986) 1279–1288.
[41] C. Stock, H.K. Grønlien, R.D. Allen, Y. Naitoh, Osmoregulation in Paramecium: in situ ion gradients permit water to cascade through the cytosol to the contractile vacuole, J. Cell. Sci. 115 (2002) 2339–2348.
[42] G. Baffou, H. Rigneault, D. Marguet, L. Jullien, A critique of methods for temperature imaging in single cells, Nat. Methods 11 (2014) 899–901.
[43] V. Brinkmann, A. Zychlinsky, Neutrophil extracellular traps: is immunity the second function of chromatin? J. Cell Biol. 198 (2012) 773–783.

Biographies

Jianguo Feng obtained his PhD in PhD in 1991 by Czechoslovak Academy of Sciences. He is a director of Institute of Parasitology, Czech Academy of Sciences and head of Laboratory of molecular biology of protists. His is interested in molecular biology of protists, evolutionary biology, mitochondrial functions and evolution.

Hanliang Zhu received his B.S. degree from Northwestern Polytechnical University (NPU) in 2017. He is currently a Ph.D. student in School of Mechanical Engineering, NPU. His research interests include microfluidics, as well as miniaturization and application of PCR systems.

Julius Lukeš obtained his PhD in PhD in 1991 by Czechoslovak Academy of Sciences. He is a director of Institute of Parasitology, Czech Academy of Sciences and head of Laboratory of molecular biology of protists. His is interested in molecular biology of protists, evolutionary biology, mitochondrial functions and evolution.

Marie Korabečná obtained her PhD in Molecular and Cellular Biology, Genetics and Virology from Charles University, Czech Republic in 2005. She became research group leader at the First Faculty of Medicine, Charles University in Prague in 2010. Her research is focused on biological functions of cell-free nucleic acids, development of PCR-based methods for clinical applications and utilization of genetic methodologies in forensic science.

Zdenka Fohlerová received her Ph.D. degree in Biochemistry from Faculty of Science of Masaryk University, Brno, Czech Republic. She is currently a junior researcher and lecturer at the Faculty of Electrical Engineering and Communication (FEEC) and Central European Institute of Technology Brno (CEITEC). Her research interests include applications of cell biology and biochemistry in the field of biosensors and microfluidics, cell – surface interactions and mechanobiology.

Ting Mei received his Ph.D. degree from National University of Singapore, Singapore, in 2000. He is currently a professor in optical engineering at Northwestern Polytechnical University, Xi'an, China. From 2000 to 2009, he was an A/professor with the Department of Electrical and Electronic Engineering, Nanyang Technological University, Singapore. From 2009 to 2013, he was a professor with the Institute of Optoelectronic Materials and Technology, South China Normal University, Guangzhou, China. From 2013 to now, he is a professor with the School of Physical Science and Technology, Northwestern Polytechnical University, Xi'an, China. His current research interest includes nanophotonics, plasmonics, ultrafast nonlinear optics and semiconductor optoelectrical material structures.

Honglong Chang received his B.S., M.S., and Ph.D. degrees from Northwestern Polytechnical University (NPU), Xi'an, China, in 1999, 2002, and 2005, respectively, all in mechanical engineering. From 2011 to 2012, he was a Visiting Associate (Faculty) with the Micromachining Laboratory, California Institute of Technology, Pasadena, CA, USA. He is currently a Professor with the Ministry of Education Key Laboratory of Micro and Nano Systems for Aerospace, NPU, where he is also the Deputy Dean of the School of Mechanical Engineering.

Pavel Neužil obtained his PhD in Electrical Engineering from Czech Technical University, Czech Republic in 1995. He joined the NPU in 2015. His research interests are advanced MEMS, microfluidics, medical devices and nanotechnology for applications such as thermal imaging (MEMS), molecular diagnostics such as portable real-time PCR (medical devices) and gecko mimicking adhesion materials (nanotechnology).